



Synthesis of polyaniline/lignosulfonate for highly efficient removal of acid red 94 from aqueous solution

Wenjing Xu¹ · Yizhen Chen¹ · Jianxun Kang² · Baojun Li²

Received: 10 April 2018 / Revised: 16 September 2018 / Accepted: 26 October 2018 /
Published online: 2 November 2018
© Springer-Verlag GmbH Germany, part of Springer Nature 2018

Abstract

Biomass is important precursor to construct environmental functional materials. Polyaniline/lignosulfonate (PANI-LS) was synthesized through one-step method and used as an adsorbent to remove acid red 94 (AR94) dye from aqueous solution. The PANI-LS was characterized using SEM, XPS, FTIR and N₂-sorption analysis. The particles of PANI-LS have been considerably changed after lignosulfonate modified polyaniline. From the batch experiment results, the solution pH plays a significant role during the adsorption. The Langmuir model well describes the adsorption data with the maximum sorption capacity of 10.56 g g⁻¹ (10,560 mg g⁻¹). Pseudo-second-order model can fit well the kinetic data obtained from batch AR94 removal experiments. The adsorption of AR94 onto PANI-LS is a spontaneous and exothermic process in nature. After adsorption, the adsorbate and adsorbent formed a gel-like composite responsible for the superior adsorption efficiency.

Keywords Adsorption · Dye · Hydrogel · Lignosulfonate · Polyaniline

Introduction

Synthetic dyes are widely used in printing, paper, textiles, leather, food and other similar industries in order to color their products. During dyeing processes, a large amount of dyes are lost resulting in colored wastewater [1]. Many of synthetic dyes possess high molecular weight, complex structures, and stability toward light, heat and oxidizing agents [2]. In water, these dyes are highly

✉ Wenjing Xu
xwj900128@126.com

✉ Baojun Li
lbjfc1@zzu.edu.cn

¹ School of Science, Jiaozuo Teachers' College, Jiaozuo Engineering Technology Research Center of Separation and Adsorption Materials, Jiaozuo 454000, Henan, China

² College of Chemistry and Molecular Engineering, Zhengzhou University, Zhengzhou 450001, Henan, China

observable even at very low concentrations, which hinder the photosynthetic rate of aquatic flora due to obstruction of light penetration [3]. Hence, removal of the dye contaminants into the environment prior to their discharge is necessary. Many treatment processes are used to address the problem, such as adsorption [4–7], chemical precipitation [8], membrane separation [9], biological processes [10], coagulation–flocculation [11], electrochemical [12], photocatalytic degradation [13]. Among these, adsorption is considered as a competitive method to remove dyes in wastewater owing to its high efficiency, economic feasibility and easy to operate [14, 15]. Many kinds of materials, for example, activated carbon [16], mineral adsorbents [17–19] and polymer [20–22] have been prepared and reported to be able to remove contaminants as adsorbents with various removal efficiency. However, it is still imperative to improve the sorption efficiency including high adsorption capacity and rate via designing novel adsorbents.

Polyaniline (PANI) is a conducting polymer and extensively studied for its easy synthesis, excellent redox properties, well-controlled electrochemistry and good environmental stability [3, 23]. In recent years, it has gained a substantial attention using bio-/conducting polymeric composite materials as adsorbent. For instance, polyanilines doped by lignosulfonate-modified carbon nanotubes [24], chitosan/polyaniline composite [25], cellulose/polyaniline composite [26] and polyaniline/bacterial extracellular polysaccharides composite [27] have been demonstrated as effective adsorbent to remove various dyes from water solution, and cross linked-chitosan-grafted-polyaniline composite [28], polyaniline/cellulose fiber composite [29], polyaniline grafted chitosan [30] and polyaniline coated chitin [31] have been reported for the adsorption of heavy metals ions from water solution.

Lignin is the second most abundant natural polymer after cellulose in the world which exists in the cell walls of terrestrial plants [32, 33]. Lignin is well known as a waste by-product in paper industries, and depending upon the pulping process, different types of lignin are obtained. Calcium lignosulfonate (LS-Ca) is usually obtained from the pulping of the acid process. LS-Ca is an aromatic three-dimensional polymer structurally, containing numbers of functional groups such as methoxyl, alcoholic hydroxyl, phenolic hydroxyl, sulfonic acid group, carbonyl and conjugated double bonds [34], which makes it and its composites adsorb many kinds of dyes.

In this paper, PANI surface was modified with LS-Ca to synthesize a biomass-based PANI-LS composite. The PANI-LS was characterized using SEM, XRD, FTIR, XPS and N_2 -sorption analysis. The adsorption capacity of PANI-LS composite on the removal of acid red 94 (AR94) from aqueous solutions was studied. The influence of various parameters, including temperature, initial pH value, contact time and initial concentration of AR94 in aqueous solution, has been investigated by batch experiment method. The maximum adsorption capacity of the PANI-LS reaches up to 10.56 g g^{-1} (equal to $10.87 \text{ mmol g}^{-1}$). After adsorption, the adsorbate and adsorbent formed a gel-like composite through electrostatic interaction, hydrogen bond and intermolecular interaction, which is responsible for the highly efficiency adsorption removal. Figure 1 shows the synthesis of PANI-LS and the proposed mechanism of AR94 removal.

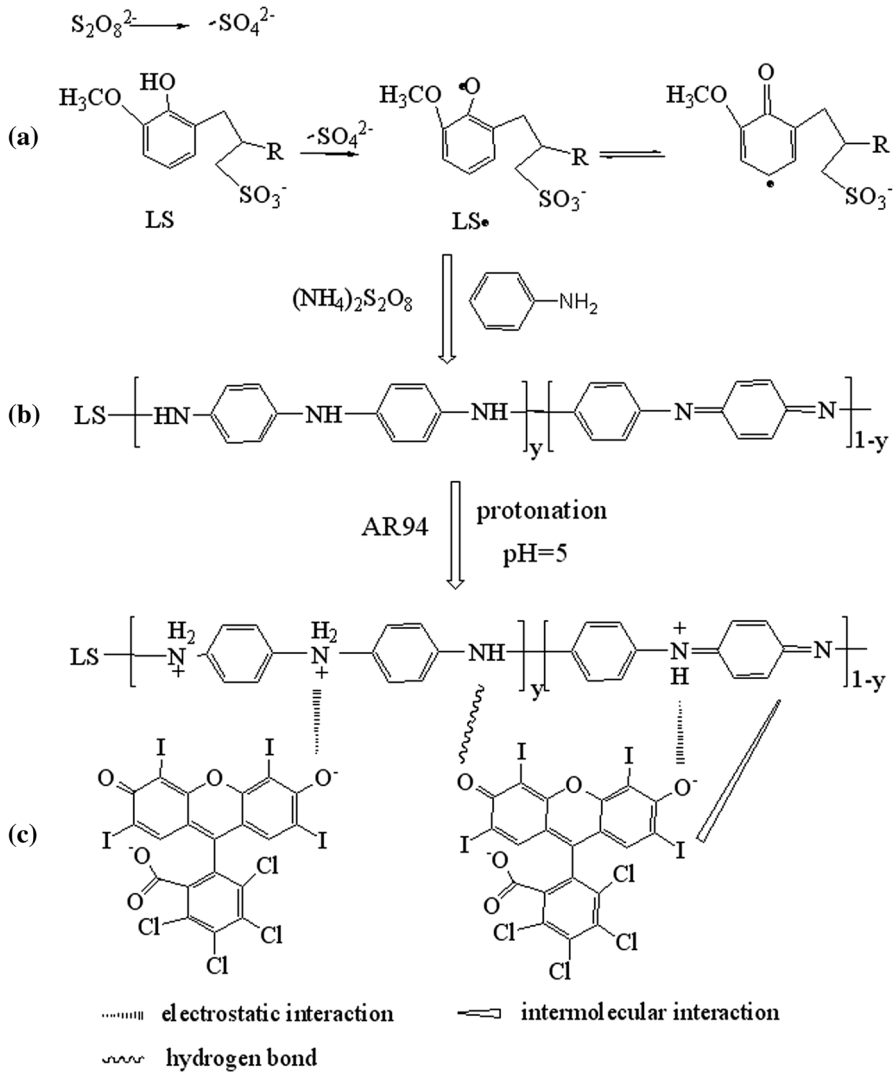


Fig. 1 Synthesis of PANI-LS, proposed mechanism of AR94 removal and the structure of **a** LS-Ca, **b** PANI-LS and **c** AR94

Experimental

Chemicals and instrumentation

Calcium lignosulfonate (96%) was purchased from Shanghai Jingcun Biochemical Technologies Co. Ltd. and was used without any further purification. The chemicals including aniline, acetone, acid red 94 (AR94), and 1,4-dioxane were supplied by Chemical Reagent (Shanghai, China). Ammonium persulfate (APS), hydrochloric

acid and sodium hydroxide were purchased from Aladdin Chemicals (Shanghai, China).

Fourier transform infrared (FTIR) spectroscopy of the adsorbents was recorded on a spectrum 100 FTIR spectrophotometer (Perkin-Elmer, USA) using a KBr disk method and scanned in the range of 4000–450 cm^{-1} . The SEM images were examined using JSM-6700F scanning electron microscopy (JEOL Ltd., Japan). The specific surface area of the samples was carried out at 77 K with the aid of volumetric adsorption analyzer (ASAP 2420, Micrometrics, USA). X-ray photoelectron spectra (XPS) of samples were explored by a PHI quantera SXM spectrometer, and according to C 1s peak (284.8 eV), the binding energies were adjusted. AR94 concentration of the test adsorbents was analyzed using a UV–Vis spectrophotometer (Lambda 35, Perkin-Elmer, USA).

Synthesis of PANI-LS

The PANI-LS composite was synthesized according to the method described in the literature [30, 35] with some alterations. Briefly, 1.0 g LS-Ca was dissolved in 100 mL of 1.0 mol L^{-1} HCl solution and stirred until totally dissolved, 30 mL of aniline monomer was dissolved in 30 mL of 1,4-dioxane to get another solution. Then, the above two solutions were mixed together. The suspension was electromagnetic stirred for 3 h to achieve the pre-equilibrium of LS-Ca and aniline monomer. After the suspensions were cooled to 0–4 °C, 40 mL of $(\text{NH}_4)_2\text{S}_2\text{O}_8$ (2.0 mol L^{-1}) water solution was dropwise added under electromagnetic stirring. The polymerizations of LS-Ca and aniline were carried out at 0–4 °C for another 12 h. The prepared products were filtrated and rinsed using acetone and distilled water for the removal of the residual free aniline monomer and $(\text{NH}_4)_2\text{S}_2\text{O}_8$. Then, lignosulfonate-modified polyaniline (PANI-LS) composite was obtained after being dried in a vacuum drying oven at 60 °C for 24 h. The polymer of polyaniline (PANI) unmodified with calcium lignosulfonate was prepared also using an identical process without the addition of LS-Ca.

Batch adsorption

The adsorption behavior of AR94 on PANI-LS composite and PANI was performed by batch equilibrium method in a conical flask. A desired amount of adsorbents was added to each flask containing 50 mL of AR94 solution. Then, the mixture was agitated in a water bath constant temperature shaker at 250 rpm for a desired time. The effect of pH was studied in the range of 3.0–11.0. Adsorption isotherms were studied using 100 mL of different initial AR94 concentration (0.500–10.00 g L^{-1}) and 50 mg of adsorbent at 25 °C and pH=5 for 24 h. Adsorption kinetics were carried out with 200 mL of AR94 concentration (3.000 g L^{-1}) and 50 mg adsorbent at 25 °C and pH=5. The samples were immediately collected at predetermined time intervals. The concentration of AR94 was calculated by calibration curve method according to Lambert's law, and the absorbance of AR94 was measured by UV–Vis

spectrophotometer at a wavelength of 548 nm. The adsorption amount (q , g g^{-1}) was calculated as:

$$q = \frac{(c_0 - c) \times V}{m} \quad (1)$$

where V (L) is the volume of the solution, c and c_0 (g L^{-1}) are the final and initial concentrations of AR94, and m (g) is the mass of adsorbent, respectively. The AR94 removal percentage was calculated as:

$$\% \text{ Removal} = \frac{c_0 - c}{c_0} \times 100 \quad (2)$$

Results and discussion

Characterization

Figure 2 shows the surface morphology evolution of (a) PANI, (b) PANI-LS, (c) AR94-loaded PANI and (d) AR94-loaded PANI-LS. It could be observed that the

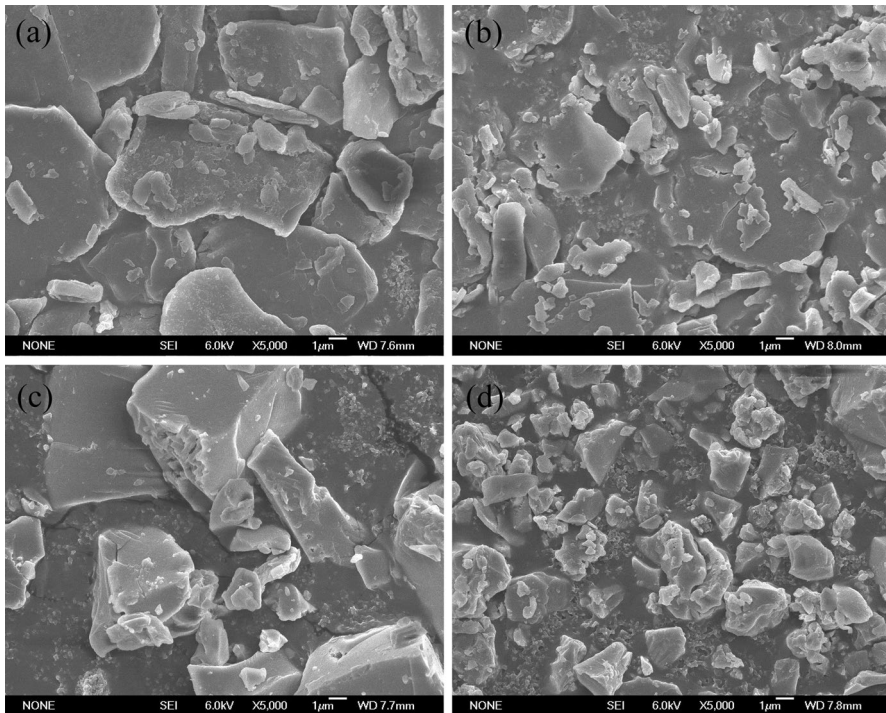


Fig. 2 SEM micrographs of **a** PANI, **b** PANI-LS, **c** AR94-adsorbed PANI and **d** AR94-adsorbed PANI-LS

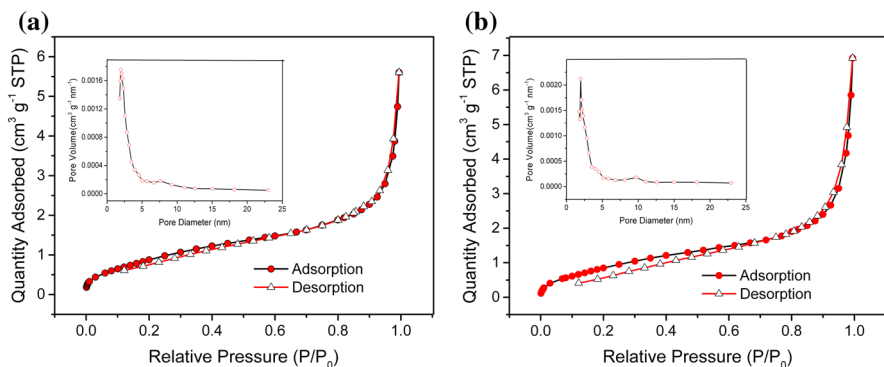


Fig. 3 Nitrogen adsorption–desorption isotherms and pore size distribution curves of **a** PANI-LS and **b** PANI

Table 1 Textural properties of PANI and PANI-LS

Adsorbent	BET surface area ($\text{m}^2 \text{g}^{-1}$)	Total pore volume ($\text{cm}^3 \text{g}^{-1}$)	Average pore diameter (nm)
PANI	3.62	0.0107	11.8
PANI-LS	3.76	0.0087	9.20

particles of PANI and PANI-LS were irregular, thin and flat, with the surface morphology smooth, and compared with the image PANI, the particles of PANI-LS were considerably reduced in size after LS-Ca modified PANI. Subsequently, it is also observed from the images (c) and (d) that after the adsorption of AR94, the particles of PANI and PANI-LS were significantly thickened and blocky in shape, which revealed that a large amount of AR94 was adsorbed by PANI and PANI-LS.

Figure 3 shows the nitrogen adsorption–desorption isotherms and the pore size distributions of prepared products. According to IUPAC classification [36], isotherms of PANI-LS (Fig. 3a) and PANI (Fig. 3b) can be categorized as type II isotherm. No obvious hysteresis loop in Fig. 3 was observed at a relative pressure of 0.4–0.9, indicating that there is no mesoporous structure in PANI and PANI-LS. Compared with PANI in Table 1, the PANI-LS showed slightly larger specific surface area and smaller pore size. The increase in surface area is favorable to adsorption.

The FTIR spectra of PANI, PANI-LS and LS-Ca are presented in Fig. 4a. The absorption peaks at 1570 and 1498 cm^{-1} are associated with the aromatic C=C stretching vibration of the quinonoid ring and the benzenoid ring. The peak at 1293 cm^{-1} is corresponding to the C–N stretching of the benzenoid unit. The C–H in-plane and out-plane bending vibration of p-disubstituted benzene ring appeared around 1138 and 736 cm^{-1} [37–40], respectively. The band in FTIR spectra of PANI-LS composite shows a slight shift compared with the prepared PANI in this study, which might be caused by the interaction between PANI and LS-Ca. From the FTIR spectrum of PANI-LS, new absorption peaks related to the aromatic ring and

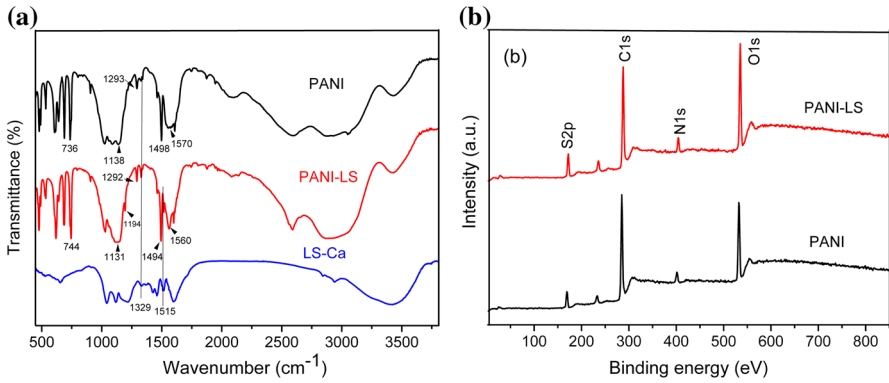


Fig. 4 **a** FTIR spectra and **b** XPS survey spectra of samples

sulfonic group [41] were observed at 1515 cm^{-1} and 1194 cm^{-1} , respectively, and the peak at 1329 cm^{-1} is enhanced, implying LS-Ca successfully modified PANI.

XPS spectrum spectroscopy technique is used also to identify and qualitatively measure the functional groups change on PANI and PANI-LS composite. As can be seen from Fig. 4b, the peak intensity of O1s at $\sim 532\text{ eV}$ and that of S2p at $\sim 170\text{ eV}$ increase due to the adding of LS-Ca, indicating LS-Ca on PANI surfaces successfully [35]. The S2p of PANI comes from ammonium persulfate in the preparation process.

Effect of pH and adsorption mechanism

The influence of pH on the adsorption of AR94 onto the PANI-LS composite and the PANI polymer was studied and is illustrated in Fig. 5a. For this purpose, the experiments were conducted with different initial pH ranging from 3.0 to 11.0 at an initial AR94 concentration of 1.500 g L^{-1} with $50\text{ mg}/100\text{ mL}$ adsorbents. From Fig. 5a, the

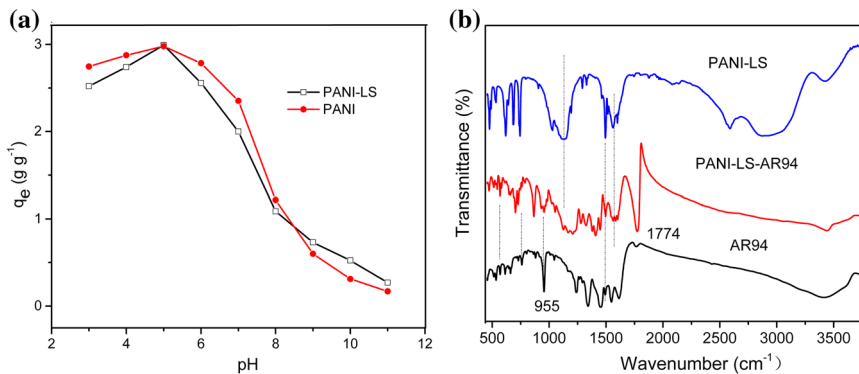


Fig. 5 **a** Effect of pH on the adsorption of AR94 by PANI-LS and PANI and **b** FTIR spectra of PANI-LS before and after adsorption of AR94

effect of pH on the removal of AR94 onto PANI-LS is basically the same as that onto PANI. The adsorption of AR94 on the two adsorbents increased with increasing pH values at $\text{pH} < 5.0$ and decreased at $\text{pH} > 5.0$. The maximum removal of AR94 on the two adsorbents was occurred at $\text{pH} 5.0$. At lower pH values, the higher AR94 removal efficiency was due to increasing H^+ ions concentration and amine groups protonation which increased the number of adsorption sites available for the AR94 sorption (Fig. 1). On the other hand, the removal of AR94 was decreased with the pH increasing. This may be because the prepared products acquired negatively charged surface with the decrease in H^+ ions concentration which enhanced the electrostatic repulsion between AR94 and the prepared products [3, 20]. Similar results were reported by other research groups [3, 20].

This property has been supported also by zero point charge studies (pH_{ZPC}). The pH_{ZPC} of the PANI-LS composite was found to be 6.0. Below the pH_{ZPC} , the surface of PANI-LS acquired positive charges and hence there was a probability of electrostatic attraction between protonated PANI-LS and the negatively charged AR94 molecules, which resulted in more AR94 adsorption from 3.0 to 6.0, while above the pH_{ZPC} value, PANI-LS was negatively charged and hence the increase in pH from 6.0 to 11.0 could result in the increase in electrostatic repulsive forces, which decreased the adsorption of AR94 on PANI-LS [42, 43].

The FTIR spectra of AR94 and PANI-LS before and after adsorption are presented in Fig. 5b. Several typical absorption bands of PANI-LS-AR94 (after adsorption AR94 by PANI-LS) can be observed, such as the absorption peaks at 1570 and 1498 cm^{-1} are corresponding to the aromatic $\text{C}=\text{C}$ stretching of the quinonoid ring and the benzenoid ring. The band at 1138 cm^{-1} is related to the absorption of $\text{C}-\text{H}$ in-plane bending vibration of p-disubstituted benzene ring from PANI-LS [37–40], and the band at 955 cm^{-1} is related to the absorption of aromatic $\text{C}-\text{O}-\text{C}$ vibration from AR94. The adsorption band at 1774 cm^{-1} ascribed to the stretching vibration of $\text{C}=\text{O}$ is enhanced obviously, which may be due to the influence of PANI-LS adsorbent on the AR94 structure during the adsorption process, resulting in the enhanced vibration of $\text{C}=\text{O}$ in AR94. Meanwhile, it also could be observed that those absorption peaks around $760\text{--}700 \text{ cm}^{-1}$ and $613\text{--}500 \text{ cm}^{-1}$ related to $\text{C}-\text{Cl}$ and $\text{C}-\text{I}$ [44], respectively, show obvious shift compared with AR94. These shifts might be caused by the interaction between PANI-LS and AR94.

Adsorption isotherms

Langmuir and Freundlich models have been widely employed to depict the adsorption equilibrium process [28]. Langmuir and Freundlich isotherms are expressed as [30]:

$$\text{Langmuir} : \frac{c_e}{q_e} = \frac{1}{q_m b} + \frac{c_e}{q_m} \quad (3)$$

$$\text{Freundlich} : \ln q_e = \ln K_F + \frac{1}{n} \ln c_e \quad (4)$$

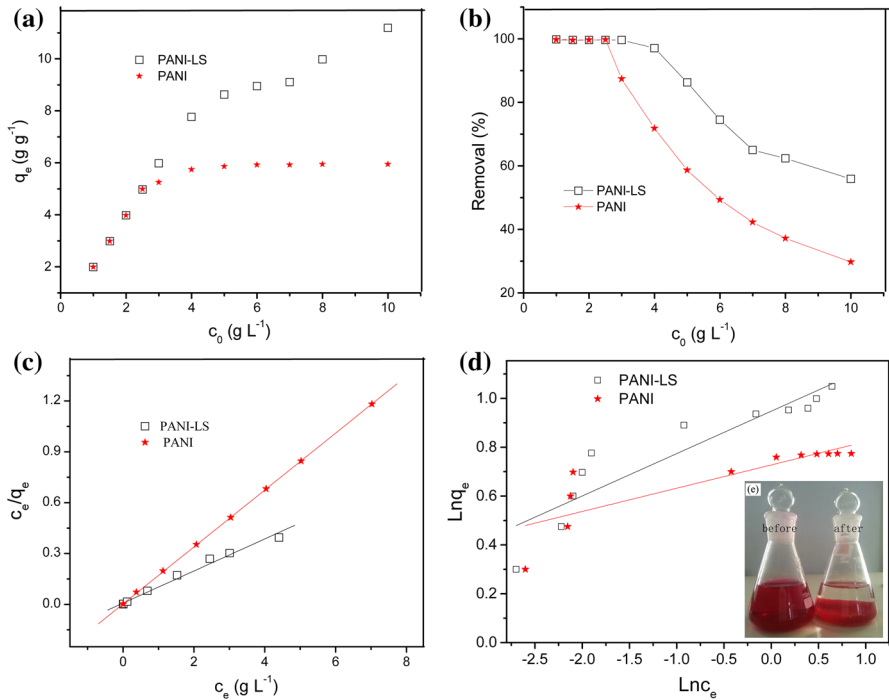


Fig. 6 Effect of initial concentration on **a** adsorption capacity, **b** removal, **c** Langmuir, **d** Freundlich adsorption isotherm for adsorption of AR94 on PANI-LS and PANI, and **e** photograph before and after adsorption of AR94 on PANI-LS

Table 2 Fitting results of adsorption isotherms by Langmuir and Freundlich models

Materials	$Q_{m\text{ exp}}$ (g g ⁻¹)	Langmuir			Freundlich		
		R_L^2	Q_m (g g ⁻¹)	B (L g ⁻¹)	R_F^2	N	K_F (L g ⁻¹)
PANI	5.947	0.9998	5.956	52.63	0.8384	10.49	5.339
PANI-LS	11.19	0.9941	10.56	12.78	0.9190	5.761	8.861

where c_e (g L⁻¹) is the equilibrium concentration of AR94, q_e (g g⁻¹) is the equilibrium adsorption capacity of AR94 onto the adsorbents, q_m represents a saturated adsorption capacity, and b (L g⁻¹) is the Langmuir adsorption constant; K_F (L g⁻¹) is the Freundlich constant which indicates the adsorption capacity, and n is the heterogeneity factor which represents the adsorption intensity.

The effect of initial concentration on AR94 adsorption capacity and removal by PANI-LS and LANI is displayed in Fig. 6a and b. The related equilibrium parameters could be calculated from the corresponding linear fitting, as shown in Fig. 6c and d, and the results are listed in Table 2. It is observed that AR94 adsorption capacity (q_e) of the two adsorbents increased and the AR94 removal was decreased

with increasing the AR94 initial concentration (c_0). The removals of AR94 were close to 100% when the initial concentrations of AR94 were below 2.5 g L^{-1} and 4.0 g L^{-1} using PANI and PANI-LS adsorbents, respectively. The higher correlation coefficient ($R^2 > 0.99$) of the Langmuir model indicates that the adsorption data of AR94 on PANI-LS and PANI fit better with the Langmuir isotherm. The obtained maximum adsorption capacity (q_m) of the PANI-LS was 10.56 g g^{-1} , which was higher than PANI (5.947 g g^{-1}). The high adsorption capacity of PANI-LS and PANI contributed to the higher content of amido and imino groups from PANI and a number of functional groups such as alcoholic hydroxyl, carbonyl, phenolic hydroxyl, methoxyl and sulfonic acid group from calcium lignosulfonate (LS-Ca) [34], which could capture AR94 molecules by electrostatic interaction, hydrogen bond and intermolecular interaction (Fig. 1). The synergy of the three aspects is responsible for the high adsorption capacity. From Fig. 6e, after adsorption, the adsorbate and adsorbent formed gel-like assembly and the removal of AR94 was close to 100%.

Thermodynamics studies

Three thermodynamic parameters, namely free energy change (ΔG°), standard enthalpy change (ΔH°) and standard entropy change (ΔS°), can be determined from Eqs. (5) and (6):

$$\Delta G^\circ = -RT \ln K \quad (5)$$

$$\ln K = -\frac{\Delta H^\circ}{RT} + \frac{\Delta S^\circ}{R} \quad (6)$$

where T (Kelvin) is the absolute temperature, R ($8.314 \text{ J K}^{-1} \text{ mol}^{-1}$) is the universal gas constant, and K (L mol^{-1}) is the sorption distribution coefficient equal to q/c_e . The effect of temperature on the AR94 adsorption onto PANI-LS and PANI is given from the plots of $\ln K$ versus $1/T$. From the slope and intercept, the ΔH° and ΔS° values were calculated.

The values of ΔG° , ΔS° and ΔH° are presented in Table 3. The enthalpy changes (ΔH°) have negatives values, indicating that the adsorption processes of AR94 on PANI-LS were exothermic. The negative values of ΔG° show that the adsorption of AR94 by PANI-LS was a spontaneous and favorable process at all temperatures of the experimental. The negative values of ΔS° indicated a decrease in the randomness at the solid–liquid interface.

Table 3 Thermodynamic parameters for the adsorption of AR94 on PANI-LS

Materials	ΔH° (kJ mol ⁻¹)	ΔS° (J mol ⁻¹ K ⁻¹)	ΔG° (kJ mol ⁻¹)			
			293 K	303 K	313 K	323 K
PANI-LS	-67.22	-154.6	-21.68	-20.64	-18.85	-17.20

Adsorption kinetics

To get a better understanding of the adsorption property of AR94 onto PANI-LS and PANI, the adsorption kinetics was studied with 3.000 g L⁻¹ of AR94 at pH 5.0, using 50 mg of PANI-LS and 100 mg of PANI, respectively. As Fig. 7a shows, a fast adsorption process was observed in the initial 60 min for PANI adsorbent and 120 min for PANI-LS adsorbent, and then the adsorption of AR94 was slow. Two kinetic models, namely pseudo-first-order and pseudo-second-order models, are used to study the adsorption kinetics behavior as shown in Eqs. (7) and (8), respectively [42].

$$\lg(q_e - q_t) = \lg q_e - \frac{k_1 t}{2.303} \tag{7}$$

$$\frac{t}{q_t} = \frac{1}{k_2 q_e^2} + \frac{t}{q_e} \tag{8}$$

where q_t and q_e (g g⁻¹) are the adsorbed amounts of AR94 at time t (min) and equilibrium time, respectively. k_1 (min⁻¹) and k_2 (g g⁻¹ min⁻¹) are the pseudo-first-order and pseudo-second-order rate constants, respectively. The kinetic parameters in the above linear models were determined by plotting $\log(q_e - q_t)$ versus t and t/q_t versus t , respectively.

The fitting results of adsorption kinetics data by pseudo-first-order and pseudo-second-order models are shown in Fig. 7b and Table 4. Compared with the correlation coefficient R^2 and the experimental adsorption capacity ($q_{e,exp}$) values, the adsorption process can be described well with the pseudo-second-order model.

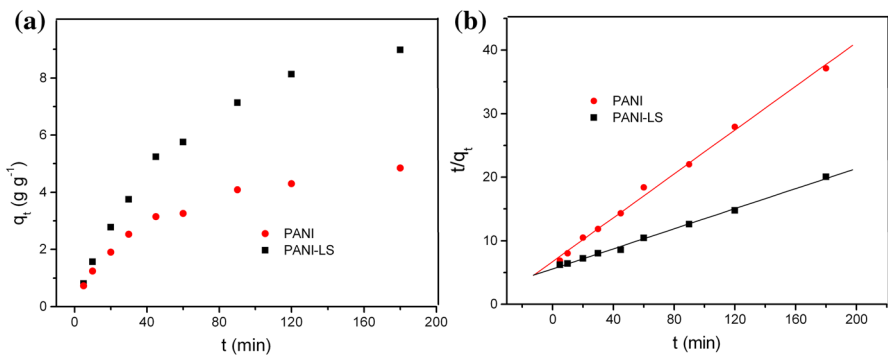


Fig. 7 **a** The effect of time on adsorption of AR94 onto PANI-LS and PANI and **b** fit of kinetic data with linear pseudo-second-order kinetic model for adsorption of AR94 onto PANI-LS and PANI

Table 4 Kinetic parameters for AR94 adsorption onto PANI-LS and PANI

Materials	Pseudo-first-order model			Pseudo-second-order model			$q_{e,exp}$ (g g ⁻¹)
	R_1^2	q_e (g g ⁻¹)	k_1 (min ⁻¹)	R_2^2	q_e (g g ⁻¹)	k_2 (g g ⁻¹ min ⁻¹)	
PANI	0.9814	4.666	8.96×10^{-3}	0.9979	5.794	4.45×10^{-3}	5.890
PANI-LS	0.9820	10.49	7.65×10^{-3}	0.9985	12.65	1.13×10^{-3}	11.89

Conclusions

In conclusion, a biomass-based PANI-LS composite was successfully fabricated through one-step technology. The existence of LS-Ca in as-prepared PANI-LS effectively increased the number of adsorption sites, and the particles of PANI-LS were considerably reduced in size after LS-Ca modified PANI. The synthetic material showed excellent removal performances for AR94. The solution pH affected the adsorption capacity, and the maximum AR94 adsorption was found at pH 5. The experimental data were well fitted by pseudo-second-order kinetics model and Langmuir isotherm. Thermodynamic parameters indicated that the adsorption of AR94 onto PANI-LS was an exothermic and spontaneous process in nature. The AR94 adsorption on PANI-LS composite was mainly attributed to electrostatic interaction, hydrogen bond and intermolecular interactions. After adsorption, the adsorbate and adsorbent formed a gel-like assembly responsible for the effective adsorption efficiency. Due to its outstanding adsorption performances and easily preparation, it could be concluded that this PANI-LS composite has great application prospects in AR94 dye wastewater treatment.

Acknowledgements This work was supported by National Natural Science Foundation of China (No. 21401168) and Foundation of Henan Scientific and Technological Committee (No. 182102210420).

References

1. Adebayo MA, Prola LDT, Lima EC, Puchana-Rosero MJ, Cataluna R, Saucier C, Umpierrez CS, Vaghetti JCP, Silva LG, Ruggiero R (2014) Adsorption of Procion Blue MX-R dye from aqueous solutions by lignin chemically modified with aluminium and manganese. *J Hazard Mater* 268:43–50
2. Zhao R, Wang Y, Li X, Sun B, Jiang Z, Wang C (2015) Water-insoluble sericin/ β -cyclodextrin/PVA composite electrospun nano-fibers as effective adsorbents towards methylene blue. *Colloids Surf B* 136:375–382
3. Ayad MM, El-Nasr AA (2010) Adsorption of cationic dye (methylene blue) from water using polyaniline nanotubes base. *J Phys Chem C* 114:14377–14383
4. Jayasanthan KH, Krishnamoorthy P, Arumugam TK, Radhakrishnan S, Vasudevan D (2017) An efficient removal of crystal violet dye from waste water by adsorption onto TLAC/Chitosan composite: A novel low cost adsorbent. *Int J Biol Macromol* 96:324–333
5. Eftekhari-Sis B, Rahimkhoei V, Akbari A, Araghi HY (2018) Cubic polyhedral oligomeric silsesquioxane nano-cross-linked hybrid hydrogels: synthesis, characterization, swelling and dye adsorption properties. *React Funct Polym* 128:47–57

6. Eftekhari-Sis B, Akbari A, Motlagh PY, Bahrami Z, Arsalani N (2018) Dye adsorption on cubic polyhedral oligomeric silsesquioxane-Based poly(acrylamide-co-itaconic acid) hybrid nanocomposites: kinetic, thermodynamic and isotherms studies. *J Inorg Organomet Polym Mater* 28:1728–1738
7. Akbari A, Arsalani N (2016) Organic-inorganic incompletely condensed polyhedral oligomeric silsesquioxane-based nanohybrid: synthesis, characterization and dye removal properties. *Polym Plast Technol Eng* 55(15):1586–1594
8. An JS, Back YJ, Kim KC, Cha R, Jeong TY, Chung HK (2014) Optimization for the removal of orthophosphate from aqueous solution by chemical precipitation using ferrous chloride. *Environ Technol* 35:1668–1675
9. Wei XZ, Kong X, Wang SX, Xiang H, Wang JD, Chen JY (2013) Removal of heavy metals from electroplating wastewater by thin-film composite nanofiltration hollow-fiber membranes. *Ind Eng Chem Res* 52:17583–17590
10. Lotito AM, Fratino U, Mancini A, Bergna G, Iaconi CD (2012) Effective aerobic granular sludge treatment of a real dyeing textile wastewater. *Int Biodeterior Biodegrad* 69:62–68
11. Al-Ani Y, Li Y (2012) Degradation of CI reactive blue 19 using combined iron crap process and coagulation/flocculation by a novel Al(OH) 3-polyacrylamide hybrid polymer. *J Taiwan Inst Chem Eng* 43:942–947
12. Yu RF, Lin CH, Chen HW, Cheng WP, Kao MC (2013) Possible control approaches of the electro-fenton process for textile wastewater treatment using on-line monitoring of DO and ORP. *Chem Eng J* 218:341–349
13. Feng Y, Feng N, Wei Y, Zhang G (2014) An in situ gelatin-assisted hydrothermal synthesis of ZnO-reduced graphene oxide composites with enhanced photocatalytic performance under ultraviolet and visible light. *RSC Adv* 4:7933–7943
14. Xu WJ, He QL, Zhang SJ, Zhang WS (2018) Adsorption of fluoride from aqueous solutions by polyacrylic acid modified with aluminium. *Polym Bull* 75:1171–1184
15. Zhu XD, Liu YC, Zhou C, Zhang SC, Chen JM (2014) Novel and high-performance magnetic carbon composite prepared from waste hydrochar for dye removal. *ACS Sustainable Chem Eng* 2:969–977
16. Zhang CM, Song W, Sun GH, Xie LJ, Wan L, Wang JL, Li KX (2014) Synthesis, characterization, and evaluation of activated carbon spheres for dibenzothiophene from model diesel fuel. *Ind Eng Chem Res* 53:4271–4276
17. Zehhaf A, Benyoucef A, Berenguer R, Quijada C, Taleb S, Morallon E (2012) Lead ion adsorption from aqueous solutions in modified Algerian montmorillonites. *J Therm Anal Calorim* 110:1069–1077
18. Mekhloufi M, Zehhaf A, Benyoucef A, Quijada C, Morallon E (2013) Removal of 8-quinoline-carboxylic acid herbicide from aqueous solution by adsorption on activated-montmorillonites. *Environ Monit Assess* 185:10365–10375
19. Zehhaf A, Benyoucef A, Quijada C, Taleb S, Morallón E (2015) Algerian natural montmorillonites for arsenic(III) removal in aqueous solution. *Int J Environ Sci Technol* 12:595–602
20. Luo X, Zhan Y, Huang Y, Yang L, Tu X, Luo S (2011) Removal of water-soluble acid dyes from water environment using a novel magnetic molecularly imprinted polymer. *J Hazard Mater* 187:274–282
21. Xu WJ, Zhang WS, Li Y, Li W (2016) Synthesis of acrylic-lignosulfonate resin for crystal violet removal from aqueous solution. *Korean J Chem Eng* 33(9):2659–2667
22. Xu WJ, Zhang WS, Li Y, Zhang SL (2016) Adsorption of methyl orange dye from aqueous solutions by acrylic composite resin chemically modified with calcium lignosulphonate. *Acta Polym Sin* 3:307–314
23. Jia YJ, Jiang JC, Sun K, Chen C (2017) Oxidation of formic acid over palladium catalyst supported on activated carbon derived from polyaniline and modified lignosulfonate composite. *J Fuel Chem Technol* 45:100–105
24. Shen Q, Mezgebe M, Li F, Dong JQ (2011) Liquids adsorption behavior and surface properties of polyanilines doped by lignosulfonate-modified carbon nanotubes. *Colloid Surface A* 390:212–215
25. Janaki V, Oh BT, Shanthi K, Lee KJ, Ramasamy AK, Kamala-Kannan S (2012) Polyaniline/chitosan composite: an eco-friendly polymer for enhanced removal of dyes from aqueous solution. *Synth Met* 162:974–980

26. Janaki V, Vijayaraghavan K, Oh BT, Shanthi K, Lee KJ, Ramasamy AK (2013) Synthesis, characterization and application of cellulose/polyaniline nanocomposite for the treatment of simulated textile effluent. *Cellulose* 20:1153–1166
27. Janaki V, Vijayaraghavan K, Ramasamy AK, Lee KJ, Oh BT, Kamala-Kannan S (2012) Competitive adsorption of Reactive Orange 16 and Reactive Brilliant Blue R on polyaniline/bacterial extracellular polysaccharides composite—a novel eco-friendly polymer. *J Hazard Mater* 241–242:110–117
28. Karthik R, Meenakshi S (2014) Facile synthesis of cross linked-chitosan-grafted-polyaniline composite and its Cr(VI) uptake studies. *Int J Biol Macromol* 67:210–219
29. Lei Y, Qian X, Shen J, An X (2012) Integrated reductive/adsorptive detoxification of Cr(VI)-contaminated water by polypyrrole/cellulose fiber composite. *Ind Eng Chem Res* 51:10408–10415
30. Karthik R, Meenakshi S (2015) Removal of Pb(II) and Cd(II) ions from aqueous solution using polyaniline grafted chitosan. *Chem Eng J* 263:168–177
31. Karthik R, Meenakshi S (2015) Synthesis, characterization and Cr(VI) uptake study of polyaniline coated chitin. *Int J Biol Macromol* 72:235–242
32. García-Mateos F, Moulefera I, Rosas J, Benyoucef A, Rodríguez-Mirasol J, Cordero T (2017) Alcohol dehydrogenation on kraft lignin-derived chars with surface basicity. *Catalysts* 7:308–322
33. Guo XY, Zhang SZ, Shan XQ (2008) Adsorption of metal ions on lignin. *J Hazard Mater* 151:134–142
34. He XJ, Xie JJ, Wei Y, Li S, Huang K, Han XQ, Zhang HY (2011) Preparation of super-absorbents composites from kaolin/sodium lignosulfonate-g-AA-AM. *Sci Silvae Sin* 47:134–138
35. Shao DD, Hou GS, Li JX, Wen T, Ren XM, Wang XK (2014) PANI/GO as a super adsorbent for the selective adsorption of uranium(VI). *Chem Eng J* 255:604–612
36. Gregg SJ, Sing KSW (1995) Adsorption, surface area and acknowledgements porosity, 2nd edn. Academic Press, London
37. Zeng XR, Ko TM (1998) Structures and properties of chemically reduced polyanilines. *Polymer* 39:1187–1195
38. Gu HB, Rapole SB, Sharma J, Huang YD, Cao DM, Colorado HA, Luo ZP, Haldolaarachchige N, Young DP, Walters B, Wei SY, Guo ZH (2012) Magnetic polyaniline nanocomposites toward toxic hexavalent chromium removal. *RSC Adv* 2:11007–11018
39. Sun YB, Shao DD, Chen CL, Yang SB, Wang XK (2013) Highly efficient enrichment of radionuclides on graphene oxide-supported polyaniline. *Environ Sci Technol* 47:9904–9910
40. Fang XH, Zhang GQ, Chen J, Wang D, Yang FL (2012) Electrochemical reduction of hexavalent chromium on two-step electrosynthesized one-dimensional polyaniline nanowire. *Int J Electrochem Sci* 7:11847–11858
41. Zhao BY, Hu KA, Fan YZ, Zhu PF, Wu RJ (2000) Infrared spectroscopic study on lignosulfonic acid and its derivatives. *Chin J Anal Chem* 28:716–719
42. Xu CM, Chen H, Jiang F (2015) Adsorption of perfluorooctanesulfonate (PFOS) and perfluorooctanoate (PFOA) on polyaniline nanotubes. *Coll Surf A Physicochem Eng Asp* 479:60–67
43. Tang L, Fang Y, Pang Y, Zeng GM, Wang JJ, Zhou YY, Deng YC, Yang GD, Cai Y, Chen J (2014) Synergistic adsorption and reduction of hexavalent chromium using highly uniform polyaniline-magnetic mesoporous silica composite. *Chem Eng J* 254:302–312
44. Chen GX (1999) Organic chemistry. Beijing Normal University Press, Beijing, pp 150–153